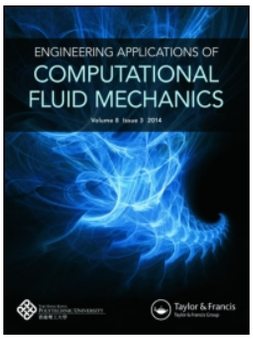

Engineering Applications of Computational Fluid Mechanics

ISSN: 1994-2060 (Print) 1997-003X (Online) Journal homepage: https://www.tandfonline.com/loi/tcfm20

Numerical simulation of the effects of building dimensional variation on wind pressure distribution

Ben Mou, Bao-Jie He, Dong-Xue Zhao & Kwok-wing Chau

To cite this article: Ben Mou, Bao-Jie He, Dong-Xue Zhao & Kwok-wing Chau (2017) Numerical simulation of the effects of building dimensional variation on wind pressure distribution, Engineering Applications of Computational Fluid Mechanics, 11:1, 293-309, DOI: 10.1080/19942060.2017.1281845

To link to this article: https://doi.org/10.1080/19942060.2017.1281845

Published online: 10 Feb 2017.

ENGINEERING APPLICATIONS OF COMPUTATIONAL FLUID MECHANICS, 2017
VOL. 11, NO. 1, 293–309
https://doi.org/10.1080/19942060.2017.1281845

Taylor & Francis
Taylor & Francis Group

Numerical simulation of the effects of building dimensional variation on wind pressure distribution

Ben Mou[a], Bao-Jie He[b], Dong-Xue Zhao[c] and Kwok-wing Chau[d]

[a]School of Civil Engineering, Qingdao University of Technology, Qingdao, China; [b]Faculty of Built Environment, The University of New South Wales, Sydney, Australia; [c]School of Environment and Architecture, University of Shanghai for Science and Technology, Shanghai, China; [d]Department of Civil & Environmental Engineering, Hong Kong Polytechnic University, Hong Kong, China

ABSTRACT

Knowledge of wind effects is of great significance in structural, environmental, and architectural fields, where excessive relevance among wind pressure, building load, and natural ventilation has been formerly confirmed. Within the scope of high-rise buildings, functions of their layout, separation and height in altering wind pressure have been inquired on purpose, while a few investigations in relation to impacts of plane dimensions have been explored. This study consequently intends to ascertain wind pressure distributions on and around various squared-shaped tall buildings by the application of Computational Fluid Dynamics techniques. To start with, models established by the Common Advisory Aeronautical Research Council (CAARC) were simulated, for the purpose of correctness comparison, and reliability verification. Hereafter, wind pressure distributing on buildings was predicted under two scenarios, namely height-width (HW) and height-thickness (HT). Results evidenced that both HW ratio and HT ratio exerted great influence on wind characteristics of buildings. Positive pressure on building surface generally varied greatly, where a narrower windward tended to suffer higher wind pressures, while a larger one was corresponding to severer negative wind effects. The thickness played little influence on altering positive wind pressure. Prominently, pressure distributed on leeward surfaces showed great differences, whereas wind effects on leeward and side surface were strengthened. Likewise, both positive and negative effects around buildings were magnified by larger widths, while negative effects became feeble along the increasing building thickness.

ARTICLE HISTORY
Received 19 October 2016
Accepted 10 January 2017

KEYWORDS
Square-shaped tall buildings; mean wind pressure; building dimensions; computational fluid dynamics; height-width scenario; height-thickness scenario

1. Introduction

Wind effects are closely associated with building load and natural ventilation in building science. Plentiful studies have been undertaken to examine wind flowing mechanism and to determine wind characteristics on buildings. Significantly, air flows around buildings have been proved susceptible and complicated according to the results of more than 50 years' investigation (Blocken, 2014), generally showing large variability with wind features, building configuration, and site characteristics. Regarding wind features, wind profiles such as exponential law, logarithmic law, and modified logarithmic law were developed on basis of regression methods, after long-term meteorological monitoring and wind tunnel tests. In current research, these models are diffusely approved and adopted, although values of several parameters are discrepant in released international wind regulations and codes (Kwon & Kareem, 2013). In the meantime, these profiles are of vital importance in turbulent models, which affect the reliability of numerical simulation in Computational Fluid Dynamics (CFD) techniques. In this sphere, scholars (Murakami & Mochida, 1988; Murakami, Mochida, & Hibi, 1987) successively executed simulation to inspect effectiveness of turbulent models such as standard k-ε turbulent model and large eddy simulation when predicting unsteady wind field around a cubic model. Although all calculated results showed good agreements with experimental data, the latter approach was much better in computing unsteady fields. To analyze wind pressure and velocity distributions on and around buildings, various k-ε models were employed to calculate three-dimensional steady fields (Baskaran & Stathopoulos, 1989, 1993; Stathopoulos & Baskaran, 1996), making great progress in wind characteristics' exploration and promoting inclusive research on wind environment.

Dating back to the 1960s, scholars embarked on rummaging relationship of surface wind pressure versus building configuration. From the viewpoint of building

CONTACT Bao-Jie He qtechhebaojie@yahoo.com

height, Baines (1963) outlined contour to acquit wind pressure distribution in conformity of results acquired in wind tunnel tests, declaring a unitary trend that maximum positive pressure was located in the vicinity of 2/3 building height rather than the top of building. To facilitate the verification tasks in experimental and numerical research, six affiliations (including Monash University (MU), University of Bristol (BU), National Physical Laboratory (NPL), National Aeronautical Establishment (NAE) and The City University (CU)) respectively measured pressure coefficients on Common Advisory Aeronautical Research Council (CAARC) standard tall building, whose achievements were afterward compiled by Melbourne (1980). These results are desirable references and foundations for future studies. Concurrently, wind pressure is vulnerable to wind direction, for evident shifts of wind pressure over different surfaces, i.e. as leeside, along with wind diversion, causing redistribution of wind pressure. Parallel to this case, Dagnew and Bitsuamlak (2014) scripted impacts of the incident condition on wind traits along CAARC model.

In the past few years, many scholars have affirmed interference effect induced by neighboring buildings, which is deemed as a sort of site impact. Original wind fields are prone to be disturbed by newly built structures, in which situations wind flows can overlap, interact, neutralize, and offset. Principal building would be totally covered merged in the negative region when building was constructed in front, resulting in both higher mean and peak negative pressures on principal buildings (Gowda & Sitheeq, 1993). Lam, Leung, and Zhao (2008) experimentally and numerically investigated wind pressure on a row of square-shaped tall buildings, reaching the conclusion that sheltered buildings sustained lower wind loads along with wind direction when comparing with isolated buildings. Kim, Tamura, and Yoshida (2011) carried out systematic experiments to examine variation of peak pressure on principal buildings subject to interference effect. It was found that peak pressure was closely bound up with subsequent arranged buildings in wind direction, building height ratio and its configuration. Notably, negative wind effects intensified dramatically as the shrinkage in interference distance. By using particle image velocimetry technique, Hui, Tamura, and Yoshida (2012) presented interference effects of various buildings with rectangular shape, where both unfavorable positive and negative peak pressures were transformed to the edges and corners of principal buildings. Yu, Xie, Zhu, and Gu (2015) made a systematic study on the interference effects between two different buildings with diverse breadth ratios and height ratios, with three kinds of configurations such as tandem, oblique, and parallel scenarios. Likewise, negative pressures were amplified greatly compared with isolated buildings in tandem and parallel scenarios.

Nowadays, it is trendy for engineers and architects to pursue singular proposals; nevertheless, wind pressure acting on these buildings with special forms is endued enormous complexity. Experimentally, scholars (Tanaka, Tamura, Ohtake, Nakai, & Kim, 2012) measured wind feature of square-shaped tall buildings with corner cut, setbacks and helical configurations, among which helical one endured better wind fields than other sorts of novelties, so that it could be utilized to significantly lower wind loads. Besides, they deduced that both overturning moments and spectral densities showed the tendency to decrease with increasing twist angle, while just small differences could be noted when the twist angle was larger than 180° Sequentially, Kim and Kanda (2013) followed with interest tapered and set-back tall buildings, exhibiting that mean pressure on the windward was almost same, while the negative one was obviously different because of the diversity in geometry. In terms of minimum pressure coefficients, set back models suffered smaller value than square prism did.

Existing studies have proven that wind pressure on buildings is in inseparable relation to adjacent structures and their geometric shapes. Therefore, it is reasonable to suppose that plane dimension of an isolated building will also exert influence on wind pressure distribution, for shelter effect undergone by the leeside varies with the enlargement of windward. However, only a few scholars have carried out research on connections between building dimensions and wind patterns. To evaluate wind effects, scholars (Lin, Letchford, Tamura, Liang, & Nakamura, 2005) drew support from a wind tunnel test, clarifying that building aspect ratio and side ratio could influence the wind load of both square- and rectangular-shaped tall buildings. Moreover, it was inadequate that general wind pressure on isolated buildings was not included for revelation and comparison. Supposing buildings were constructed in a hilly terrain field, others (Li, Sun, Huang, Chen, & Wei, 2010) looked into relationships between wind loads on various shaped buildings and their aspect ratios as well as side ratios, and they drew the conclusion that wind loads on rectangular-shaped buildings were more vulnerable to aspect ratios and side ratios than those on circular-shaped models.

Generally, a few efforts have focused impact of building plane dimension on wind pressure distribution. Consequently, this article is devised to respond to this issue, through numerically predicting wind pressure on and around rectangular-shaped tall buildings. Consistent with previous studies (Braun & Awruch, 2009; Elshaer, Aboshosha, Bitsuamlak, El Damatty, & Dagnew, 2016; Zhang & Gu, 2008; Huang, Li, & Xu, 2007),

three-dimensional steady wind field will be calculated with the assistance of RNG k-ε turbulent model in CFD technique. The succeeding section will basically outline several numerical items that may affect both correctness and effectiveness of numerical simulation, such as computational domain, grid arrangement, boundary conditions, solution methods, and solver control. Meanwhile, full information of scenarios including height-width (HW) and height-thickness (HT) will be presented, respectively. To guarantee the validity and reliability of our research, Section 3 will to compare computed results with experimental results of the CAARC standard models. Section 4 and Section 5 show holistically compared wind pressure distributions on and around tall buildings in both HW and HT scenarios. Overall, the anticipation of this investigation is to inform engineers and architects with basic understanding in relation with natural ventilation in both indoor and outdoor environments.

2. Numerical simulation: parameters and scenarios

To establish appropriate numerical models and obtain accurate computed results, many factors should be taken into consideration, such as computational domain, grid generation, boundary conditions, solver setting, and residual control. Pressure prediction will suffer some issues in stability, accuracy, reliability as well as calculated quantity, if parameters are not well considered. Main settings in model establishment are outlined as follows.

2.1. Computational domain and grids

Concerning computational domain of models, various guidelines have been proposed. Scholars including Tominaga et al. (2008) recommended that distances around models should be long enough to ensure the full development of wind fields (He, Yang, & Ye, 2014), where upstream and downstream zones were at least five times and ten times the buildings height. Blocken (2015) reviewed urban physical factors that lower accuracy and reliability of CFD simulation and came up with corresponding scientific recommendations. Huang et al. (2007) presented computational domains for tall buildings and this investigation showed computational domain in Figure 1. On accordance with these suggestions, computational domains in this article were totally sketched as $X \times Y \times Z = 900\,\text{m} \times 900\,\text{m} \times 500\,\text{m}$. The length of upstream domain was 300 m, more than 1.5 times of building height H. The blockage ratio was less than 5%, which could eliminate wall effect when conducting wind-related numerical simulation in atmospheric boundary layer (Barlow, Rae, & Pope, 1999; Liu,

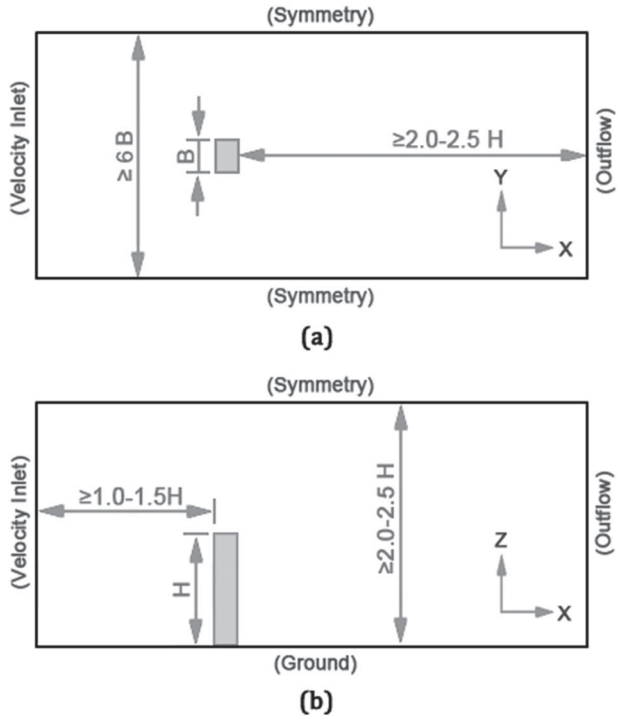

Figure 1. Computational domain and boundary conditions: (a) Top view; (b) Side view.

Niu, Kwok, Wang, & Li, 2010; Yuan, Ng, & Norford, 2014). Although some work suggested that blockage ratio should not exceed a recommended value as 3% (Montazeri & Blocken, 2013; Tominaga et al., 2008).

Grid quality and quantity determine computation time and results' precision to a large extent. Based on the pre-processing module ICEM CFD 14.0 (ANSYS, 2011), we selected a hexagonal structured grid technique and local mesh refinement approach, aiming to greatly reduce the computation time and improve precision of prediction results. As presented in Figure 2, grids around building were approximately 15 times denser than other regions, where minimum grid was all partitioned approximately 0.0054H, meeting resolution requirements (Montazeri & Blocken, 2013). According to recommendation in ANSYS FLUENT 14.0 (ANSYS, 2011), the volumes of minimum and maximum cell were 5.67m^3 and $6.1 \times 10^3\text{m}^3$, respectively. Additionally, it is worth noting that total grid number of each model varies because of distinct dimension of building in a fixed computational domain.

2.2. Boundary conditions

Type of inlet was velocity-inlet during numerical simulation in ANSYS FLUENT 14.0 (Figure 1). The height of every building was quite high, so that we adopted power law wind profile to fit actual atmospheric boundary layer,

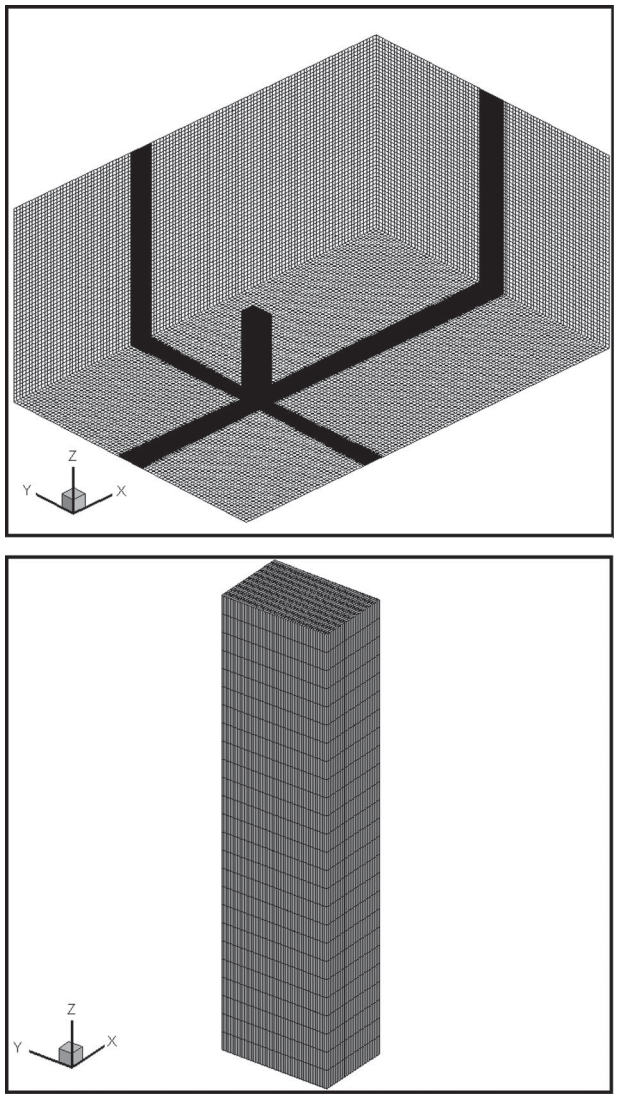

Figure 2. Grid generation: (a) Overall grid distribution; (b) Refined grid on building surface.

as given in Eq. (1).

$$\frac{U(z)}{U_H} = \left(\frac{z}{z_H}\right)^{\alpha} \tag{1}$$

where $U(z)$ means the wind velocity at a specific height of z, U_H is wind velocity at building height of 182.88 m, α represents ground roughness exponents, set as 0.27 according to Architectural Institute of Japan (AIJ, 1996). The wind profile is given in Figure 3.

Turbulent intensity I is mainly deemed as a significant factor to determine flow characteristics of wind separation. Therefore, it is interpreted for sharp results (Figure 3), which is calculated by the following equation.

$$I = 0.1\left(\frac{z}{z_G}\right)^{-\alpha-0.05} \tag{2}$$

CFD simulation in this study adopted Realizable $k-\varepsilon$ turbulent model, therefore, parameters including turbulent kinetic energy and turbulent dissipation rate should be taken into consideration. When it comes to the turbulent kinetic energy k (as shown in Figure 3), it has close relation to turbulent intensity I and wind speed U. Therefore, turbulent kinetic energy k could be predicted according to Eq. (3), where a is a constant depending on standard deviations of turbulent fluctuations (Montazeri & Blocken, 2013; Ramponi & Blocken, 2012; Tominaga et al., 2008). As indicated in previous studies, the value of constant a could be set as 0.5, 1.0 and 1.5, and in this numerical simulation $a = 1.0$ (Tominaga et al., 2008). Furthermore, the turbulence dissipation rate ε (as shown in Figure 3) is expected to be calculated on the basis of Eq. (4), in which l means turbulence integral length scale. It was tested by some scholars in the wind tunnel test (Huang, Luo, & Gu, 2005; Obasaju, 1992) and its value was set as 0.58 m in some CFD simulations (Huang et al., 2007). In addition, C_u is an empirical constant in numerical model, equal to 0.09 (Tominaga et al., 2008).

$$k(z) = a(I(z)\cdot U(z))^2 \tag{3}$$

$$\varepsilon = C_u^{3/4}\cdot\frac{k^{3/2}}{l} \tag{4}$$

This study was designed to simulate steady and incompressible flows with a unified density, the Outflow boundary conditions were chosen in all models. This, in others words, has assumed that wind flow has fully developed without any disturbing at the outlet of the computational domain. Regarding the buildings and ground surface, the wall boundary conditions were given. The wall was set as stationery and with no-slip shear condition, ensuring that no velocity occurred between the moving flow and internal faces.

2.3. Solution method and control

Numerical simulation was performed on the ANSYS FLUENT 14.0, where the SIMPLE pressure–velocity coupling algorithms put forward by Spalding (1972) were adopted. It is recognized that the Second-Order Upwind Scheme could facilitate higher accuracy computational results based on the Taylor series expansion (Barths, Antoni, & Peters, 1998). Therefore, it was selected to discretize momentum, turbulent kinetic energy, and turbulence dissipation rate. In addition, when absolute values were less than 10^{-4} for x, y velocity, 10^{-4} for z velocity and 10^{-4} for continuity, k and ε, the convergence of numerical computation was achieved.

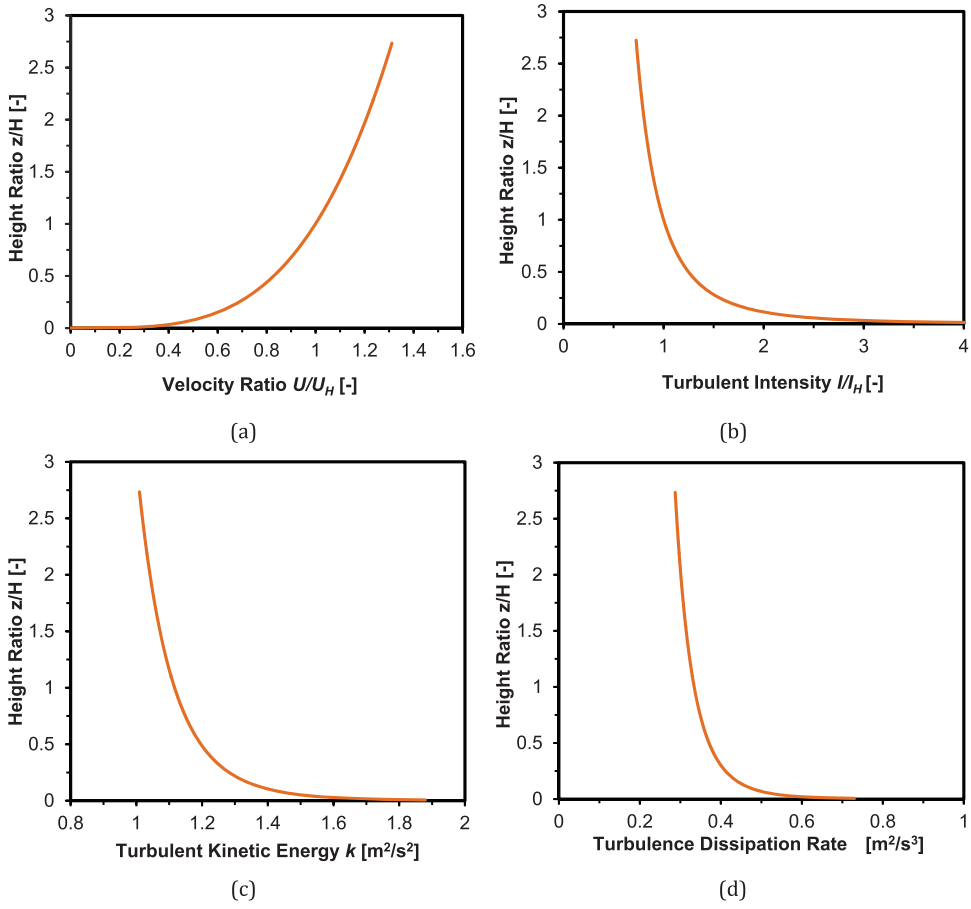

Figure 3. Profiles of different parameters: (a) Wind velocity profile; U (b) Turbulent intensity; I (c) Turbulent kinetic energy k; (d) Turbulence dissipation rate ε.

2.4. CAARC model validation and scenarios

As evidenced by previous researchers (Huang et al., 2007; Montazeri & Blocken, 2013; Tominaga et al., 2008), results derived from CFD simulation are always affected by various factors. To validate both effectiveness and accuracy of this simulation, we started with established CAARC tall building models. Calculated mean wind pressure coefficients under four kinds of wind directions (including 0°, 30°, 60°, and 90°) at the height of 2H/3 were firstly compared with experimental data given by six affiliations. We again mention basic parameters of six above wind tunnel tests in Table 1. Note that great differences exist in their parameters (Melbourne, 1980). Therefore, large discrepancies were found in their experimental results. Meanwhile, comparisons were not ideal but still useful to evidence the corrections of present CFD simulation (Huang et al., 2007).

Mean wind pressure coefficient C_p is calculated based on Eq. (5).

$$C_p = \frac{P - P_0}{\frac{1}{2}\rho U_H^2} \tag{5}$$

where P means the pressure exerted on the building surface, P_0 is the static pressure at reference height, ρ is air density with common value of 1.225 kg/m^3, U_H is wind velocity at the reference height of building, and $U_H = 7.43m/s$ at $z = 182.88m$.

Table 1. Basic parameters of original wind tunnel tests.

	Dimension		Velocity		Blockage ratio	
	m	Length ratio	m/s	Wind profile	%	Turbulence intensity
CU	0.76 × 0.60	1/690	15	0.23	3.90	0.080
BU	2 × 1	1/500	12	> 0.30	2.00	0.100
MU	2 × 2	1/400	30	0.25	1.30	0.090
NAE(a)	9.1 × 9.1	1/400	15	0.28	0.06	0.090
NAE(b)	9.1 × 9.1	1/400	15	0.28	0.06	0.100
NPL	2.7 × 2.1	1/240	18.3	0.25–0.30	2.50	0.085

After careful validation, two series of rectangular-shaped building models were created to investigate the influence of building dimension on their wind characteristics. Models could be divided into two scenarios, including height-width (HW) scenario and height-thickness (HT) scenario, and specific information is outlined in Tables 2 and 3, respectively. It is worth noting that the current computational domain was unified; therefore, blockage ratio would be different when building dimensions varied in length and width. While blockage ratios were all equal to 1.63% due to the same windward in HT scenario, blockage ratios saw great variation from 1.63% to 4.88% in HW scenario. Definitely, however, all blockage ratios were less than the threshold of 5% (Barlow et al., 1999; Liu et al., 2010; Yuan et al., 2014). Furthermore, both HW ratio and HT ratio were distinct, from 1.52 to 4.57, along with variation in their plane dimensions.

Table 2. Rectangular-shaped tall buildings: HW scenario.

	Building dimension ($L \times W \times H$)		Computational domain ($X \times Y \times Z$)	Blockage ratio
Model	M	HW	m	%
R-A-1	40 × 40 × 182.88	4.57	900 × 900 × 500	1.63
R-A-2	60 × 40 × 182.88	3.05	900 × 900 × 500	2.44
R-A-3	80 × 40 × 182.88	2.29	900 × 900 × 500	3.25
R-A-4	100 × 40 × 182.88	1.83	900 × 900 × 500	4.06
R-A-5	120 × 40 × 182.88	1.52	900 × 900 × 500	4.88

Table 3. Rectangular-shaped tall buildings: HT scenario.

	Building dimension ($L \times W \times H$)		Computational domain ($X \times Y \times Z$)	Blockage ratio
Model	M	HW	m	%
R-B-1	40 × 40 × 182.88	4.57	900 × 900 × 500	1.63
R-B-2	40 × 60 × 182.88	3.05	900 × 900 × 500	1.63
R-B-3	40 × 80 × 182.88	2.29	900 × 900 × 500	1.63
R-B-4	40 × 100 × 182.88	1.83	900 × 900 × 500	1.63
R-B-5	40 × 120 × 182.88	1.52	900 × 900 × 500	1.63

3. Numerical results and validation: CAARC model

CAARC model respectively subjected to wind effects from four directions were investigated to guarantee the validity of this simulation, where computed results at the 2H/3 were presented in Figure 4. It was indicated that mean coefficients generally shared consistent patterns to

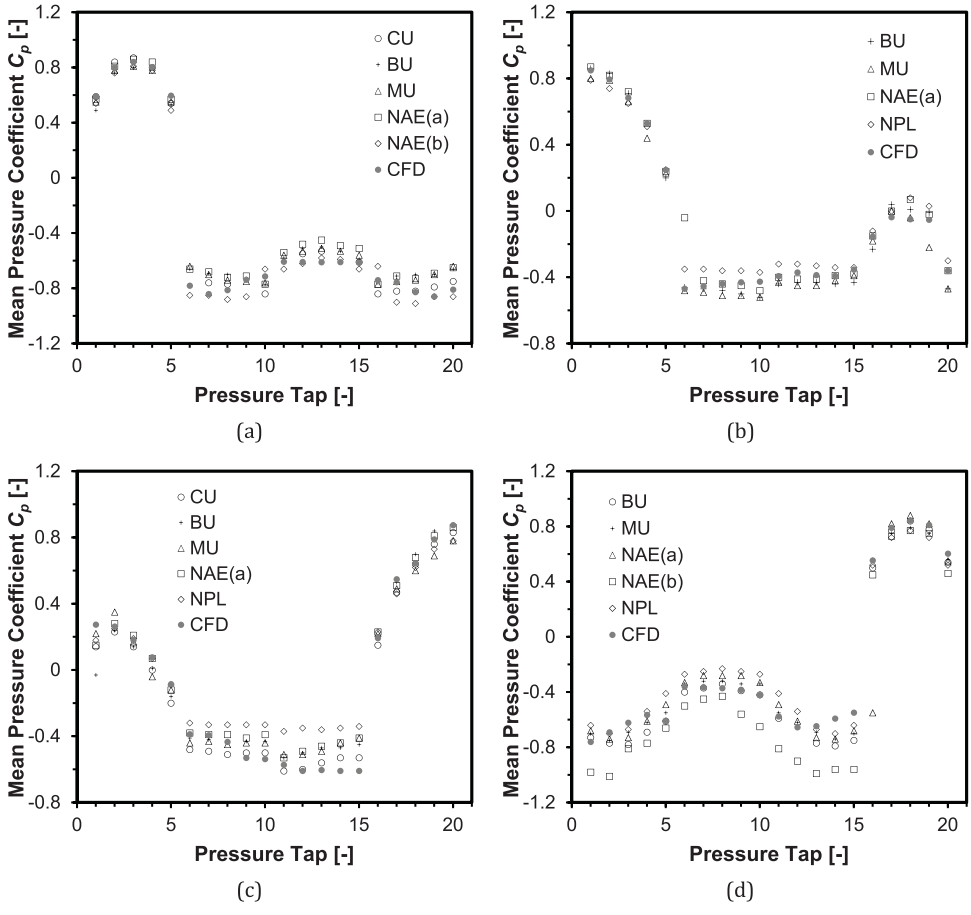

Figure 4. Comparison of computed wind pressure coefficients and experimental data under different wind directions: (a) 0°; (b) 30°; (c) 60°; (d) 90°.

previous results, although some obvious discrepancies could be observed. In the case of 0°, coefficients on windward side showed favorable agreements with existing experimental results, where the maximum value at the midpoint is 0.84. On the leeward surface, calculated data overall underwent less variation compared with experimental results. For wind pressure on side walls, computed results likewise saw the best agreement with the NAE(b) model when all numerical data fell in the total scope of measurements.

This section had also compared computed results and experimental results at the premise of 30°, 60°, and 90°. It was obviously noted that numerical results followed basic trends performed in original wind tunnel tests. As shown in Figure 4(b), numerical simulation maintained its highest precision from tag 1 to tag 5, while it under-predicted wind pressure from tag 6 to tag 15, in spite of 20% larger than NPL models in terms of absolute value. CFD model showed larger discrepancies when simulating wind pressure between tag 12 and tag 14. Likewise, under the situation of oblique wind angles (presented in Figure 4(c)), wind pressures were exactly estimated in positive pressure zones, while negative pressures were somewhat over-predicted (from tag 11 to tag 15). Perpendicularly, simulated results showed same trend, although back surface was somewhat lower in absolute value (Figure 4(d)). Herein, through comparison between computed results and experimental data based on Eq. (6), it is reasonable to draw the conclusion that computed errors are basically less than 20%, consistent with results reported by Obasaju (1992).

$$\text{Absolute error} = \left| \frac{C_{p\ CFD} - C_{p\ tunnel}}{C_{p\ tunnel}} \right| \times 100\% \qquad (6)$$

where $C_{p\ CFD}$ represents mean wind pressure coefficient calculated via CFD techniques;

$C_{p\ tunnel}$ is the results obtained via wind tunnel test at CU, BU, MU, NAE(a), NAE(b), and NPL.

4. Effects of dimension on surface pressure coefficients

Windward (front surface 0–1), side wall (1–2, 3–4) and leeward (back wall 3–4) are presented in Figure 5(a). To investigate wind characteristics of on and around various squared-shaped tall buildings with different plane dimensions, we sliced wind pressure coefficients at the height of 2H/3, H/2 and H/3, as shown in Figure 5(b). Furthermore, wind pressures at the central axis and trisection line in both HW and HT scenarios were studied, the arrangement of central axis and trisection line as shown in Figure 5(c).

Additionally, mean pressure coefficients on building surface were not collected continually, while a unified interval was settled on different walls. Specifically, at the different heights (H/3, H/2 and 2H/3), data was collected every one meter. Along the height of buildings, data was collected every five meters on windward surface and leeward surface, while data was gathered every two meters.

4.1. General features

To reveal wind characteristics on building surface, models (including R-A-5, R-A-1/R-B-1, R-B-5) with the maximal width, intermediate thickness and width, and the maximum thickness were selected, as shown in Figure 6. When making a comparison between model R-A-5 and model R-A-1, it was noted that positive pressure coefficients varied greatly. On the front wall (windward side), pressure of the latter one generally increased along the height, while the former one witnessed both decrease in

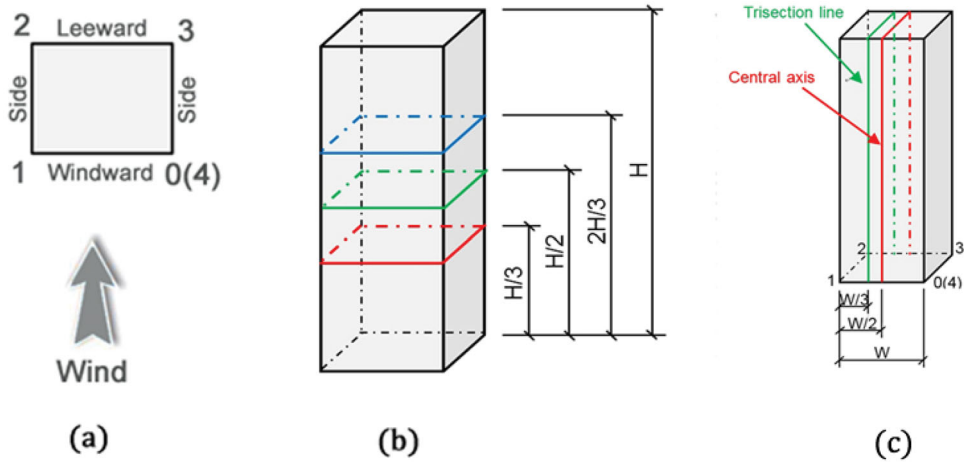

Figure 5. Configuration of special lines: (a) Building surface; (b) Different height levels; (c) Central axis and trisection line.

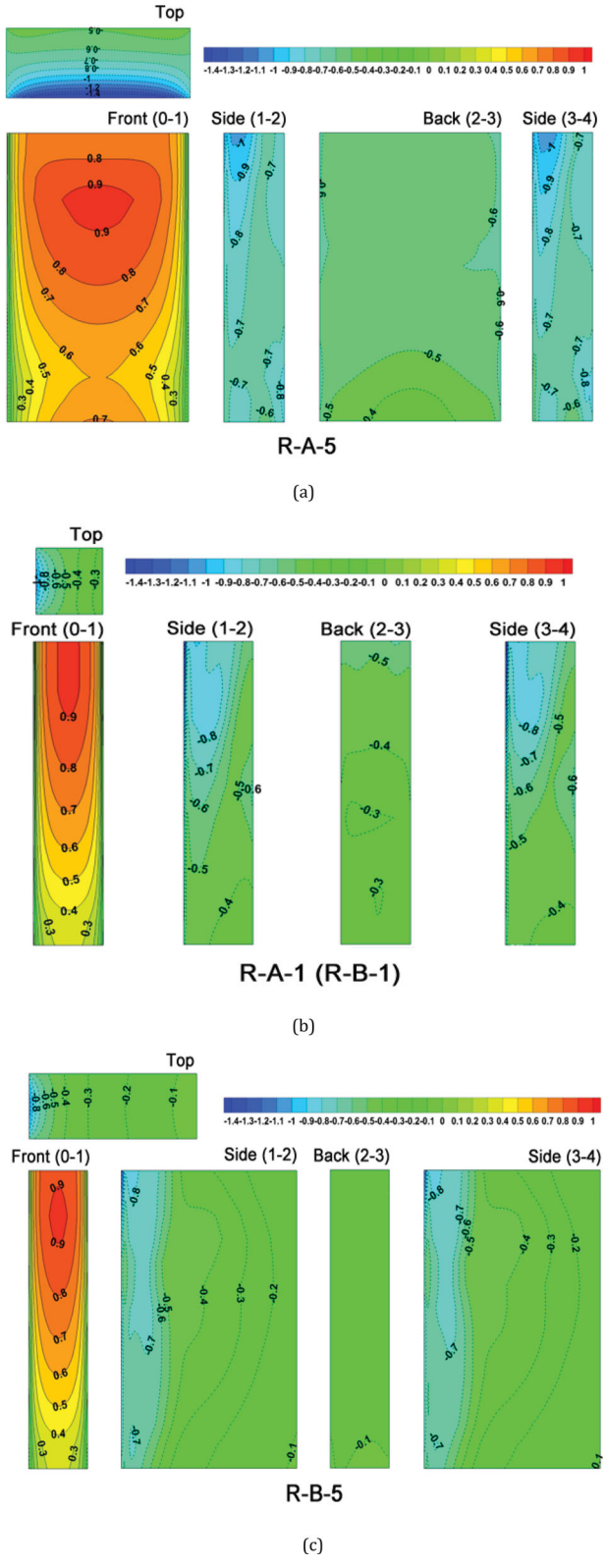

Figure 6. Contour of wind pressure coefficients against on building surface: (a) R-A-5; (b) R-A-1 (R-B-1); (c) R-B-5.

0–0.2H and 0.8H-H. Maximum coefficient zone were circled by line 0.8 and 0.9 in case R-A-5. However, pressure coefficients were semi-open and maintain this trend to the top of model. It is therefore easy to conclude that a narrower windward surface is more likely to suffer higher wind pressures.

On the contrary, side surfaces (including 1–2 and 3–4) were prone to expose to higher wind pressures, when windward surfaces were wider. As for case R-A-5, wind pressure coefficient scopes 0.8–1.0 around the top-left in figures, while largest values were just in the range of 0.7–0.8 around the same place. If values were not taken into consideration, nevertheless, trend displayed by isobaric lines was overall consistent. For the leeward surface, wind effects in case R-A-1 evenly magnified by building height, ranging between −0.5 and −0.3. The wall was mainly covered by a larger value of 0.6 in mean coefficients C_p in case R-A-5, although building height augmented its pressure to a certain extent. Note that absolute value of maximum negative pressure on the top of R-A-5 was larger than 1,4, while that in R-A-1 just reached 0.8, indicating wind effects of the latter one is much flabbier. Overall, it is concluded that building with larger width suffers relatively weaker positive pressure effects, while subject to more intense negative wind effects.

For case R-B-1 and case R-B-5, they shared most similarities in positive pressure, as shown in Figure 6(b) and (c). However, the largest coefficient zone circled by 0.9 for R-B-1 was larger, with its semi-open traits. With regard to negative pressure, top surfaces enjoyed same pressure distribution, while pressure of R-B-5 increased to −0.1 due to its long distance in thickness. On the side surfaces, wind pressures in the same horizontal zones were generally same, and relatively lower pressures near the back walls on R-B-5 were mainly consistent with additional thickness. It was worth highlighting that wind pressure distributed on leeward surfaces showed great differences. In R-B-5, pressure coefficients show fluctuation of 0.1, while pressure fluctuation in R-B-1 reached 0.4. Smaller fluctuation in former one might be caused by the fact that after gradually passing long distance along the side surface, air flow was forwarded and turned steady, without intense wind effect on back wall. In general, building thickness has little influence on windward side, but longer distance in thickness will reduce wind effects.

4.2. Height-width ratio: a category

4.2.1. Different height levels

Figure 7 presents the distribution of mean wind pressure coefficients C_p for buildings with various widths, when surfaces are respectively sliced at 2H/3, H/2, and H/3. As shown in Figure 7(a), positive mean C_p on the windward surface (0–1) increased along the width of wall, from case R-A-1 to case R-A-4. In current study, positive mean C_p was no longer doughty, globally going down

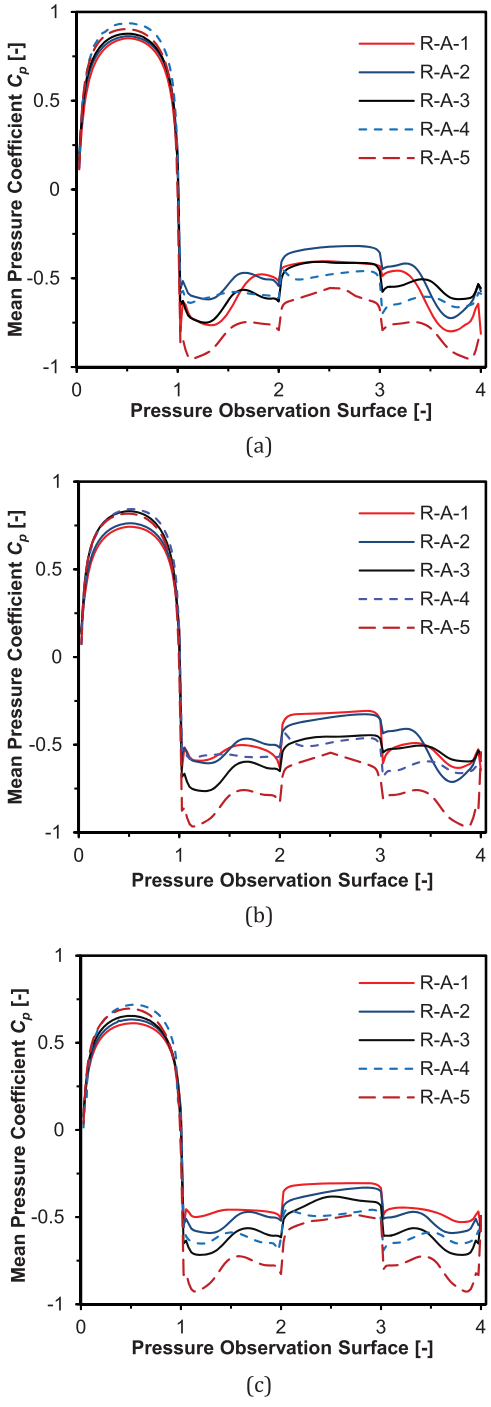

Figure 7. Mean wind pressure coefficients at different heights in HW scenario (a) z = 2H/3; (b) z = H/2; (c) z = H/3.

when windward surfaces persistently broadened. Compared with case R-A-4, maximum value for case R-A-5 presented is just 0.904, roughly decreasing by 3.5%. Concerning variation of C_p at H/2 and H/3, similar trends are easily found in Figure 7(b) and (c), although their values have a marked trend of decline.

Compared with the biggest difference of 0.085 in positive C_p, negative wind pressures exerting on the leeward sides experienced larger disparities. At the same location, the largest differences were more than 0.31, 0.34, and 0.23 for 2H/3, H/2, and H/3, respectively. In general, absolute values of wind pressure coefficients increased dramatically, as the width of leeward wall, especially, increasing from 0.321 (R-A-2) to 0.556 (R-A-5). Additionally, it was interesting to note that wind pressures on a specific leeward wall were quite stable, lying in a horizontal line in given figure, except case R-A-5. This may indicate that properties of wind fields changed along the width of leeward wall, since an isolated building seemed to be a wall when width-to-thickness was magnified. Therefore, the middle area formed weak zone with suffering feeble wind suction, exposure to smaller wind pressure than zones close to borders.

Wind pressures on side surfaces experienced great fluctuations, so as to make a slow transition from side to back wall in negative pressure. On side walls, negative pressures adjacent to the windward were larger than that near to leeward wall. Interestingly, lines composed by mean C_p (1–2 and 3–4) were symmetrical, where the symmetrical points were located on its central line (corresponding to 1.5 and 3.5) in Figure 7. This might be related to the wind flow separation adjacent to windward and reattachment near to leeward wall (Richards & Hoxey, 2006). It was not evident to conclude general trend for R-A-3 undergoing relatively even wind pressure. On that basis, absolute value of negative average C_p showed a trend of growth as the increase of wall width, among which the maximum negative C_p of R-A-5 are all at the scrutiny of −0.95.

4.2.2. Central axis

To holistically investigate wind distribution under different HW ratios, mean C_p at the central axis along the building façade were extracted, as demonstrated in Figure 8. Regarding wind pressures applied on the windward surface, Figure 8(a) exhibits a consistent trend that wind pressure coefficients rise along with the height of measurement points, reaching its maximum value at the scrutiny of 0.8H of established model and then dropping sharply to zero at the top of buildings. Meaningfully, mean C_p decreased from a specific value near the ground to its minimal value around 0.1H–0.2H. For case R-A-5, while mean C_p at the height of 5 m (0.027H) was 0.692 followed by 0.614 at the height of 25 m (0.137H), its value increased to 0.928 at 0.766H and declined to approximately zero at the top.

When exploring the influence of HW ratios, wind pressure generally enlarged when wall width increased. Most apparently, original value of C_p for R-A-1 near the ground was about 0.343, rising to 0.669 for R-A-4, almost doubled. After the mentioned minimal values in the range of 0.1H–0.2H, pressure fluctuations between

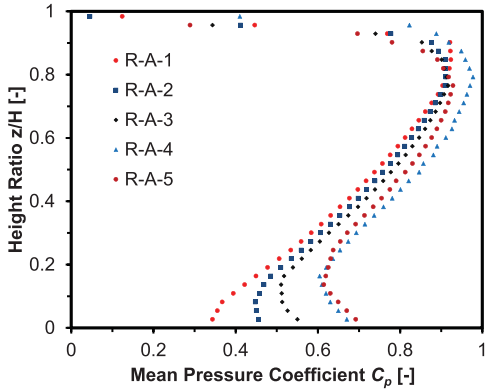

(a)

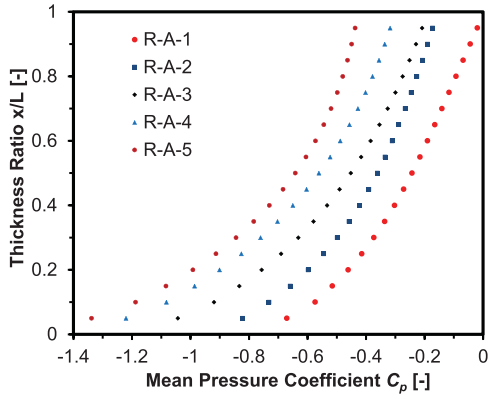

(b)

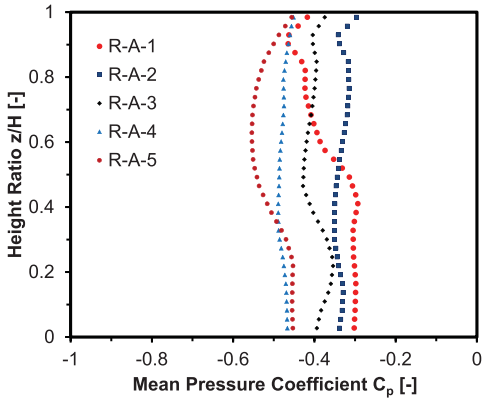

(c)

Figure 8. Mean wind pressure coefficients at the central axis line in HW scenario: (a) Front surface; (b) Top surface; (c) Back surface.

all models diminished, ranging 0.911 to 0.976 at 0.80H, with just 0.055 larger than the lowest value. Near the top, surface pressure coefficients, however, showed a trend of decrease along with the breadth of buildings. For the most part, mean C_p of case R-A-5 were smaller than that of case R-A-4, although a pressure coefficient line was located at the right in Figure 8 (a).

Wind effects on top surface turned inconspicuous along the direction of air flow, as shown in Figure 8(b). In case R-A-5, for instance, the absolute value of mean pressure coefficients C_p considered a drop from 1.338 around the windward wall to only −0.438 close to back wall. Variations in this scenario were closely connected to intense wind separation action and reattachment phenomenon, which afterwards alleviated wind effects. As a whole, pressure coefficient lines were arranged from left to right in order, indicating mean C_p on the top surface decreasing evenly along the HW ratios, where the interval between each model was about 0.15.

With regard to wind pressure action on the leeward wall, the range of variation was relatively narrow, between −0.30 and −0.55 (as indicated in Figure 8(c)). Wind pressures uniformly followed the trend that pressures steadily and evenly decreased, meaning that driving forces turned strong, as per the growth in width, when HW ratios ranged from 1.83 to 3.05. At the same time, pressure coefficients for specific models were quite stable along the building height, which was consistent with the pressure exerted on the surface of multi-storied buildings (Montazeri & Blocken, 2013). In addition, it should be highlighted that wind pressures of case R-A-1 suffered great fluctuation when the height was above 0.5H, roughly following the trend mentioned above. Compared with the lower-half-section, coefficients C_p were smaller, which might be caused by wind suction from top and side surfaces. This could only be realized at a narrow width. As for the case R-A-5, its wind pressure coefficients were the smallest among all cases, led by the widest leeward, corresponding to the largest wind driving effects.

4.2.3. Trisection line

In addition, wind characteristics at the trisection line were also investigated and calculated results are presented in Figure 9. Similar to mean C_p distribution trend at the central axis line, wind effects became strong (shown by absolute values of C_p) along the width of models. However, some differences had been recognized in wind pressure distribution on various surfaces. To start with, wind pressures on the top surface were generally much less than that at the central axis line. For case R-A-5, minimum coefficient at the central axis line was marked as −1.339 near the ground, while it reduced to −1.425 at the trisection line at the same height. It was understandable that the leeward wall suffered from stronger wind suction force when measured locations were more likely to approach the side walls. Therefore, mean C_p at the trisection lines on the back surface were conformably smaller than that at the central axis lines. Note that pressure coefficients of R-A-5 were totally lower than that of case R-A-4.

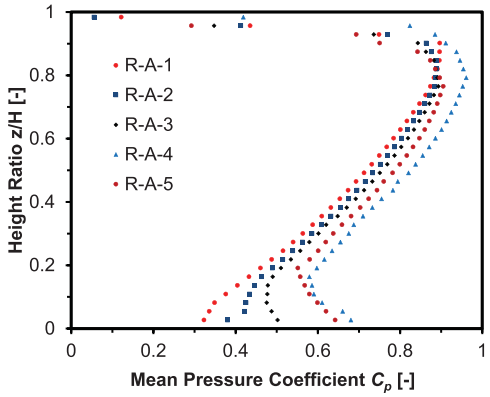

(a)

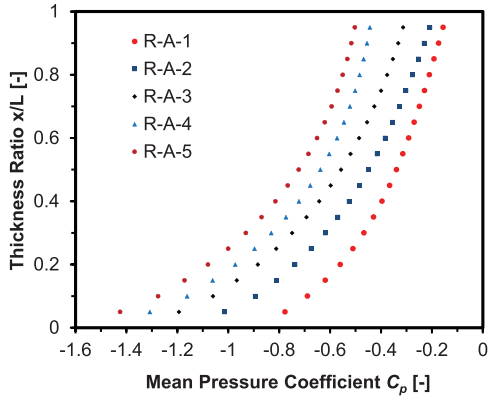

(b)

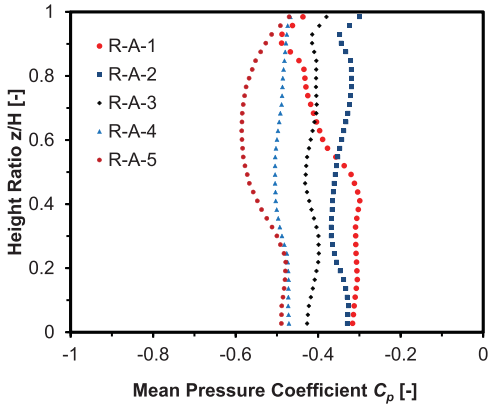

(c)

Figure 9. Mean wind pressure coefficients at the trisection line in HW scenario: (a) Front surface; (b) Top surface; (c) Back surface.

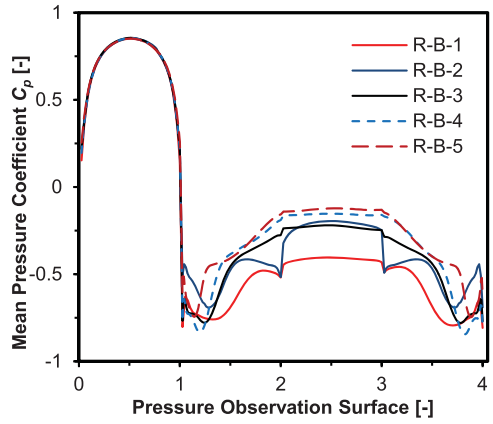

(a)

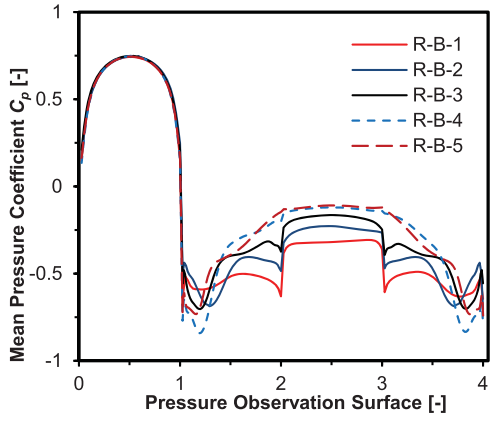

(b)

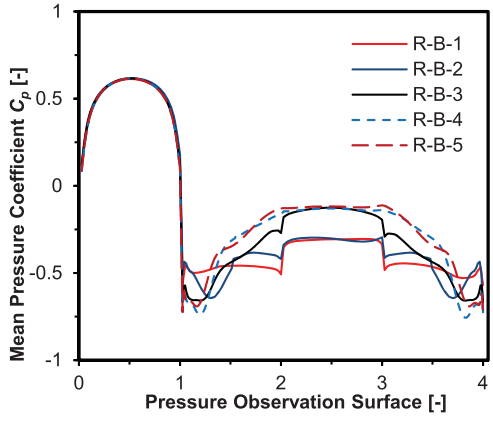

(c)

Figure 10. Mean wind pressure coefficients at different heights in HT scenario (a) z = 2H/3 (b) z = H/2 (c) z = H/3.

4.3. Height to thickness ratio: B category

4.3.1. Different height levels

Effects of HT ratios on the variation of mean wind pressure coefficients C_p had been well studied, at the same horizontal and vertical lines employed in HW scenario. Similarly, mean C_p around buildings at various heights (Figure 10) had also enclosed ostrich-shaped lines, just like the coefficients shown in Figure 7, at first sight. As shown in Figure 10, coefficient lines in the range of 0–1 coincided, indicating that HT ratios imposed little influence on positive pressure applied on the windward wall. Positive values presented in Figure 10(a), nevertheless, were generally larger than that given in Figure 10(b), followed by positive coefficients of Figure 10(c). In terms of the mean C_p at the central point of windward surface, namely 0.5 in pressure observation surface, values were around 0.855 at the height of 2H/3, while values reduced

to approximately 0.745 at H/2 and then 0.615 at H/3. As a consequence, we concluded that wind pressures positive correlatively varied with building height.

When it comes to pressure dragging the back wall of buildings, it is effortless to observe that wind suction tends to weaken as the growth of building thickness. At the height of 2H/3, coefficients C_p of case R-B-1 fell into the range of −0.404 to −0.446, while mean C_p of case R-B-5 were in the range of −0.122 to −0.141, considerably less than former models. Meanwhile, coefficient gaps between neighboring models showed a tendency of drop, since lines for case R-B-4 and case R-B-5 were likely to overlap. This phenomenon was more clearly evidenced at H/2 and H/3, respectively. That is to say, response of wind pressure to ever increasing thickness would turn smaller.

Wind pressure imposing on both side surfaces were quite complex, specified by several intersecting lines in the range of 1–2 and 3–4. Similar to trends in HW scenario, lines were symmetry on the basis of abscissa at 1.5 and 3.5, respectively. Adjacent to the back wall (surface 1.5–2.0 and surface 3.0–3.5), mean C_p became small as the increase of building thickness, for coefficient lines were upward from R-B-1 to R-B-5. In addition, gaps between successive lines turned small, illustrating that impacts of HW ratio were not clear when it reached a threshold. For wind pressures on surface 1.0–1.5 and surface 3.5–4.0, they were greatly relevant to building height. Note that absolute values of coefficient for case R-B-1 were larger than that of other case at the height of 2H/3, while values rank at middle level at H/2 and bottom level at H/3. This was corresponding to ever up-floating R-B-1 lines among three figures in Figure 10.

4.3.2. Central axis

Mean C_p have been extracted at the central axis of windward surface, which are presented in Figure 11(a). Obviously, wind pressure lines for various models overlapped, showing that wind pressures on building façades were not disturbed by building thicknesses. At the same time, it could observe that mean C_p achieved their maximum value 0.920 around 0.83H.

On top surfaces (Figure 11(b)), coefficient lines were arranged from left to right in order. That means mean C_p decreased with the increase in building thickness. For the measurement points adjacent to back surfaces, wind pressure in case R-B-1 was −0.273, while its value in case R-B-5 is −0.037. Additionally, it was interesting to note that the values of pressure coefficients were almost −0.935 at the first tested points. More importantly, HW ratios had an apparent effect on wind pressure when thicknesses were relatively small. Contrasting both case R-B-1 and R-B-2, we realized that mean C_p of the former one was approximately 0.1 lower than that of the latter one. When comparing both case R-B-4 and R-B-5, however, it was liable to know the latter one was just 0.02 higher than the former one in value. Therefore, wind effects on top surface were gradually feeble along with thickness.

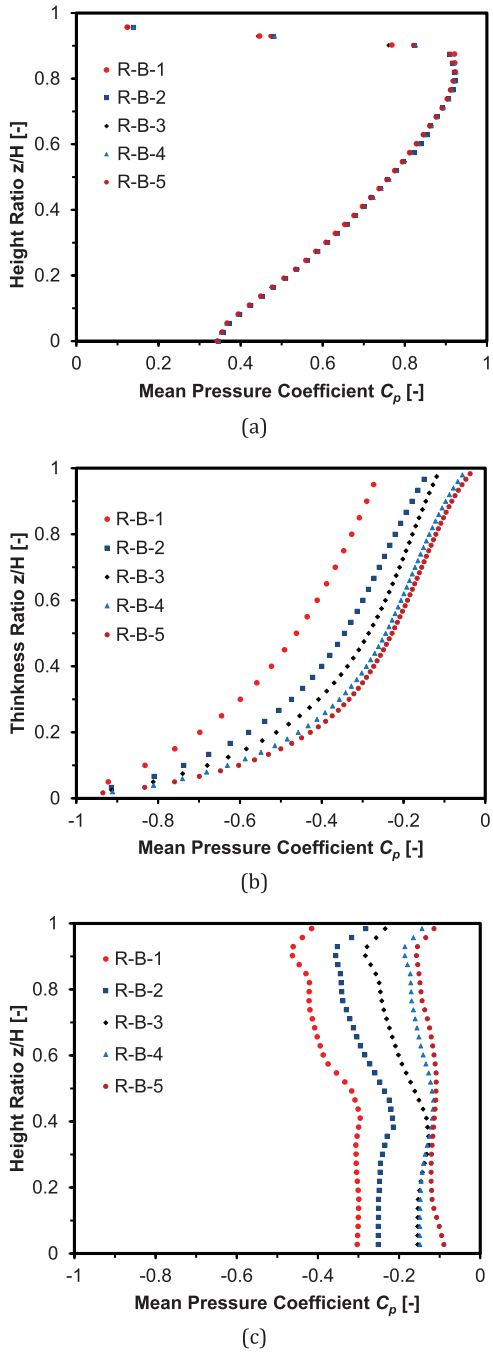

Figure 11. Mean wind pressure coefficients at the central axis line in HT scenario: (a) Front surface; (b) Top surface; (c) Back surface.

Figure 11(c) presents mean wind pressure coefficients C_p on leeward sides of various models. Along with the building height, wind pressures had not seen great fluctuations, among which the largest one happened in

model R-B-1, ranging from −0.296 to −0.463. Interestingly, coefficient line for case R-B-5 seemed like a straight line with the smallest fluctuation of just 0.07. Referring to influence of HW ratios, wind pressures declined when building thicknesses were becoming larger, since coefficient lines were fixed from left to right. In particular, all calculated data for R-B-5 higher than −0.15, about 0.30 larger than that of R-B-1. This might mean ever elongating in thickness had formed a guarded section to weaken wind effects at the central axis of leeward wall.

4.3.3. *Trisection line*

Wind characteristics at the trisection lines of all models were concerned. As demonstrated in Figure 12(a), mean C_p also showed no difference along with variation of building thickness. Compared with positive pressure at the central axis, pressure exerted at trisection line is a little bit lower, of which the maximum value was about 0.894 around 0.83H. On the top surfaces (Figure 12(b)), mean C_p showed same trend as the coefficients at central axis, also witnessing slightly smaller values like positive

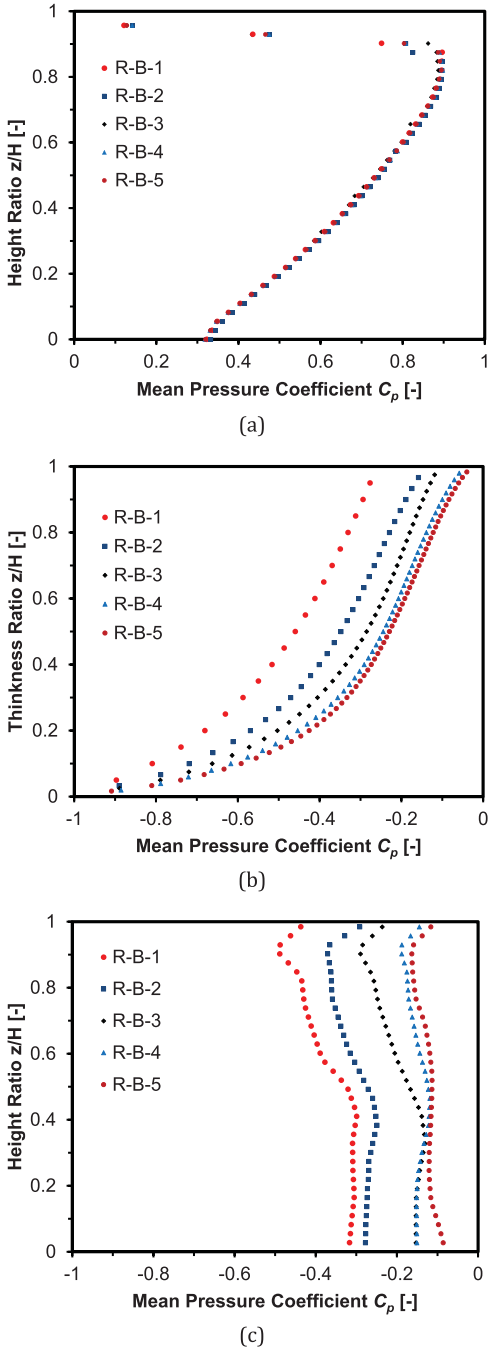

Figure 12. Mean wind pressure coefficients at the trisection line in HT scenario: (a) Front surface; (b) Top surface; (c) Back surface.

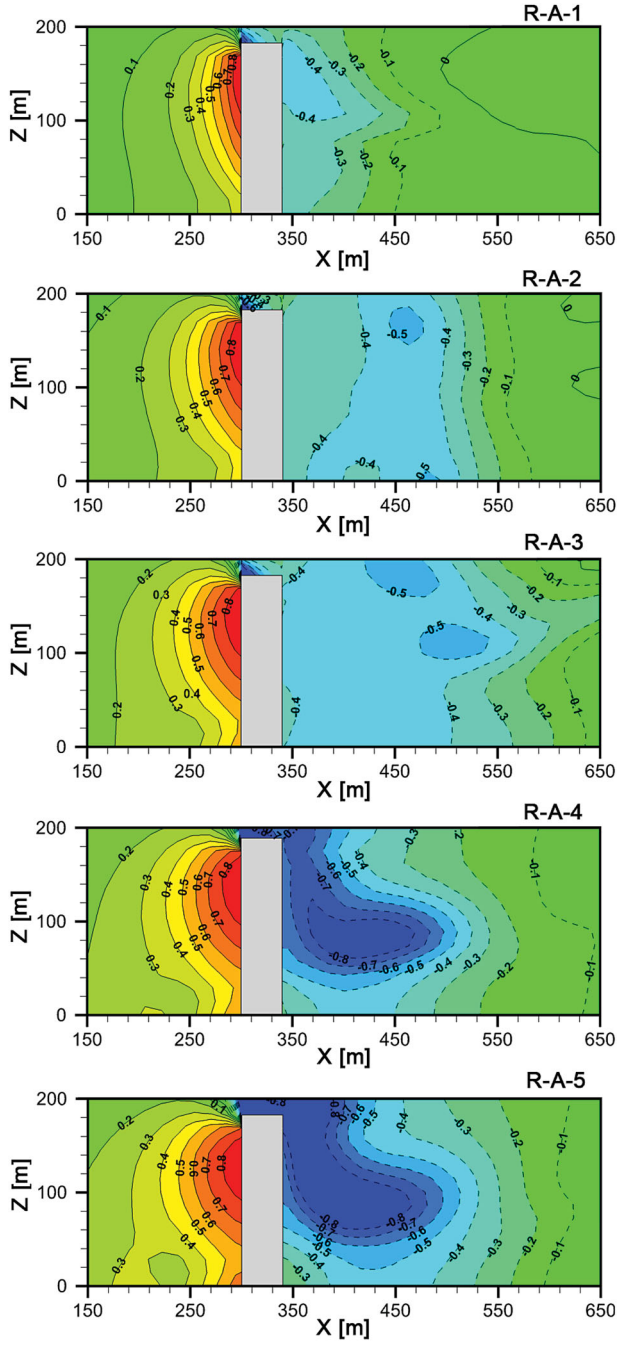

Figure 13. Wind pressure coefficients around buildings at Y/2 in HW scenario.

pressure. For case R-B-1, coefficient value of measurement point near back wall was −0.273 at central axis, while the value reduced to −0.276. Nevertheless, this indicated that more intense wind effects occurred when away from central axis. Similarly, wind characteristics at the trisection line (Figure 12(c)) on the leeward surface were generally identical with that at central axis with only mildly smaller value.

5. Wind pressure distribution around buildings

5.1. Height-width ratio: a category

Apart from wind pressure on buildings, wind pressure distributions around buildings were also investigated, at the specific height of 2H/3 and Y/2 of computational domain. Figure 13 demonstrates wind effects at the Y/2 of the computational domain. Focusing on the area of 0–150 m from front surface, we figured out that distributions of positive wind pressure were basically identical, while some small fluctuations existed in their values. Near the wall, positive pressure zone with a specific value augmented along the width of models. Apparently, the area encircled by line 0.8 increased from R-A-1 to R-A-5. At the same time, line 0.1 was easily observed in Figure 1, while line 0.2 was severed by the vertical axis in R-A-5. Around the back of buildings, negative pressure distributions were also quite vulnerable to building dimensions (Tsang, Kwok, & Hitchcock, 2012). Generally, strong wind effect zones formed by specific coefficient line were successively enlarged. In R-A-1, positive wind pressure could be noted away from the back wall (marked by 0), while pressure turned to be negative at the same location in R-A-5 (marked by −0.1). In another aspect, maximum wind effects that were larger than 0.8 in its absolute value only distributed on the top of R-A-1, while the top one spread continually and merged large zones in the back areas around R-A-5, for the increasing effect in blocking.

In addition, wind pressure distributions around building had been analyzed at the height of 2H/3, as shown in Figure 14. Intuitively, both maximum positive and negative zones stamped by crimson and dark blue colors were respectively accounted for largest proportions in model R-A-5, while R-A-1 witnessed the smallest, indicating wind effects were intensified by the increasing width. As a consequence, it is concluded that wind effects have all been magnified by larger width around both front and back sides of buildings.

5.2. Height to thickness ratio: B category

Figure 15 shows pressure characteristics of HT scenario, where positive coefficients distributed in front areas share a great deal of similarities. This indicates that building thickness still has little influence on positive wind effects around tall buildings. However, back areas presented caught many differences in negative wind pressure. Specifically, pressure coefficients in case R-B-1 ranged from −0.4 to 0, and the −0.4 zone occupied certain proportion around the top-back wall. Wind effect degraded along the thickness of models, which was certified by the narrower range of 0– to 0.1. Around top surfaces, few imparities emerged due to a great difference in building thickness. Additionally, Figure 16 shows that wind pressure distributed at 2H/3 follows same trend as concluded at the y = Y/2 of computational domain. Wind pressures around the front of buildings indicated

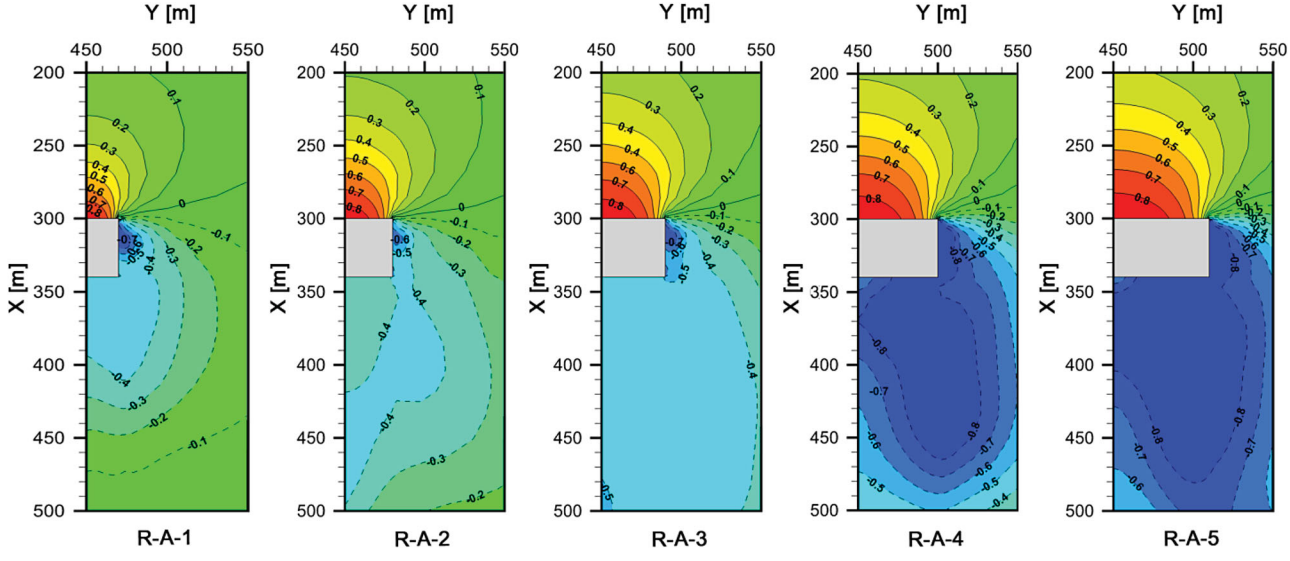

Figure 14. Wind pressure coefficients around buildings at the height of 2H/3 in HW scenario.

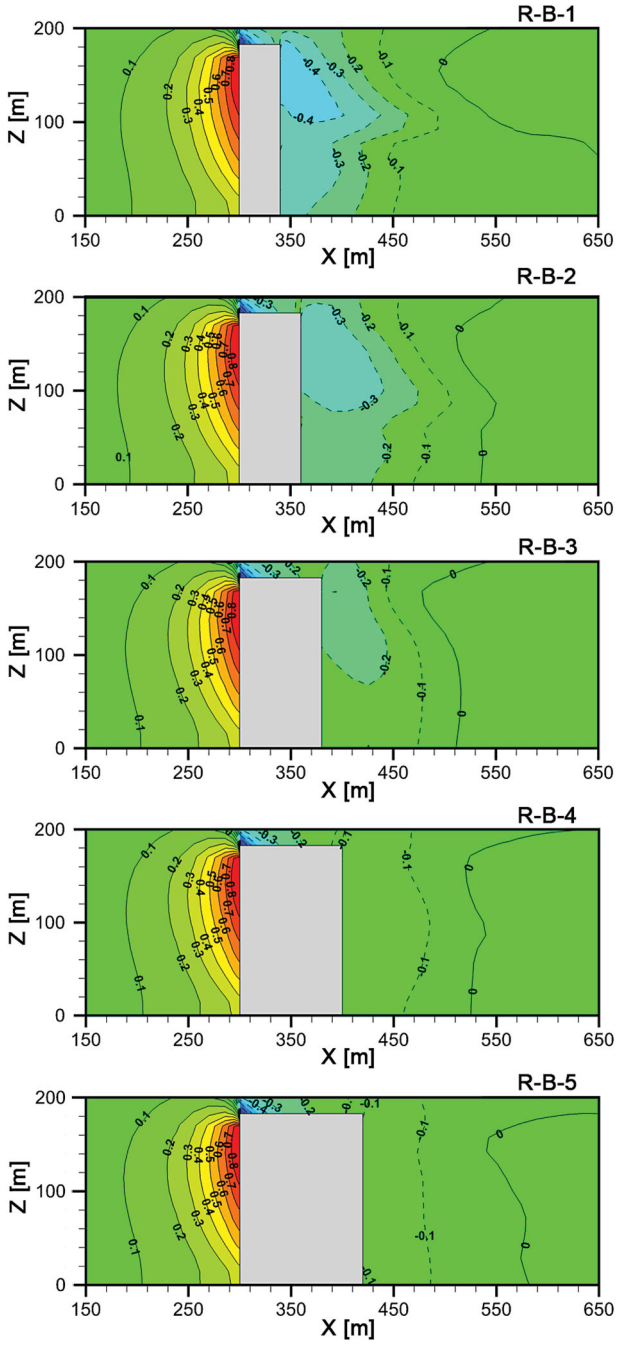

Figure 15. Wind pressure coefficients around buildings at Y/2 in HT scenario.

no difference among all models, but negative pressures fell into the range of −0.4 to −0.1, generally meaning that wind effects diminished with the increase in thickness.

6. Conclusions and remarks

This article has systematically investigated mean wind pressure on and around various square-shaped tall buildings for the consideration of dimension effect. Results have evidenced that both HW ratio and HT ratio exerted great influence on wind characteristics of buildings. In general, positive pressure on building surface varied greatly. Concretely, a narrower windward was more likely to suffer higher wind pressures, and a larger one was corresponding to a severer negative wind effect. The thickness played little influence on altering positive wind pressure. Prominently, pressure distributed on leeward surfaces showed great differences, although wind effects receded along their thicknesses. In HW scenario, positive mean C_p on the windward had been magnified at the same height, while these coefficients globally went down when windward surfaces persistently broadened. On the leeward side, negative wind pressure had also strengthened since absolute values of coefficients increased dramatically with building widths. Side surfaces witnessed great fluctuations in wind pressure among all cases. Along the building façade, datum clustered at feature positions expresses a trend of rise, reaching its maximum at the scrutiny of 0.8H and then dropping sharply to zero at the top of models. On the flank and top surface, wind effects in both positive and negative aspects were generally amplified when building width increased. Leeward side beard steadily and evenly declining pressure, conversely meaning that driving forces turned strong in specific HW ratio within the range of 1.83 and 3.05. HT ratio brings small effects on positive pressure in both horizontal and vertical directions, while significant influence on negative pressure. Wind suction on the leeward surface tended to be weakening as growth in building thickness. Mean C_p on the side surface became small in pace with building thickness, impacts of HW ratio were not clear when the thickness reached a threshold. Wind effects gazed upon top and leeward surfaces were gradually feeble with thickness. Wind effects around buildings had all been magnified by larger width around both the front and back sides of buildings. However, building thickness exerted less influence on positive pressure, while negative wind effect became feeble along with its value.

We devise this research to investigate the connections among various planar shapes and wind effects, and only rectangular-shaped scenario has been highlighted in this article. Future work will therefore focus on other sorts of planar shapes, such as oval and cross scenarios. Moreover, one shortcoming of this research may lie in application of numerical simulation, since the wind tunnel test is still the secure choice for many scholars and engineers. Accordingly, the work presented in article will favorably accept experimental inspections.

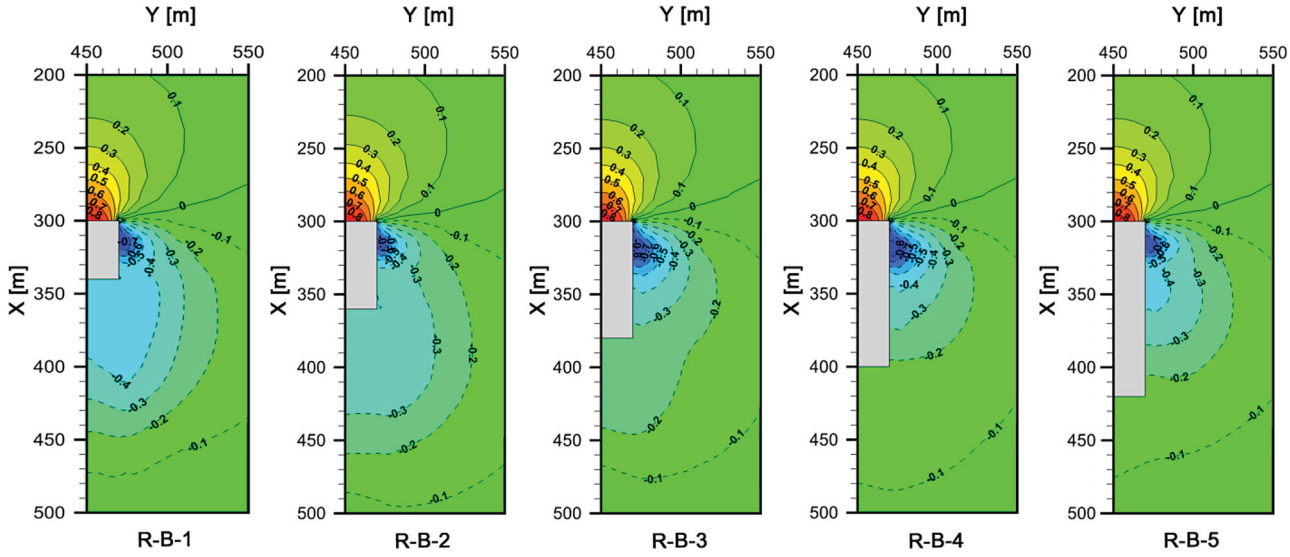

Figure 16. Wind pressure coefficients around buildings at the height of 2H/3 in HT scenario.

Disclosure statement

No potential conflict of interest was reported by the authors.

Funding

This article is financially supported by National Natural Science Foundation of China with the project No. 51278259. Meanwhile, it is funded by the Shandong Province Taishan Scholar Advanced Disciplinary Talent Group Project; Shangdong Province Young and Middle-Aged Scientists Research Awards Fund (ZR2016EEB38); Innovation Fund for Postdoctor in Shandong Province (201601017) and Qingdao Applied Research Funding (2016194).

References

AIJ. (1996). *AIJ recommendations for loads on buildings*. Tokyo: Architectural Institutes of Japan.

ANSYS. (2011). *14.0. User's and theory guides*. Canonsburg, PA: ANSYS Inc.

Baines, W. D. (1963, June). Effects of velocity distribution on wind loads and flow patterns on buildings. In *Proceedings of the symposium on wind effects on buildings and structures* (Vol. 1, pp. 26–28). Teddington: National Physical Laboratories.

Barlow, J. B., Rae, W. H., & Pope, A. (1999). *Low-speed wind tunnel testing* (3rd ed.). New York: John Wiley & Sons.

Barths, H., Antoni, C., & Peters, N. (1998). Three-dimensional simulation of pollutant formation in a DI diesel engine using multiple interactive flamelets (No. 982459). SAE Technical Paper, 1–13.

Baskaran, A., & Stathopoulos, T. (1989). Computational evaluation of wind effects on buildings. *Building and Environment*, *24*(4), 325–333.

Baskaran, A., & Stathopoulos, T. (1993). Numerical computation of wind pressures on buildings. *Computers & structures*, *46*(6), 1029–1039.

Blocken, B. (2014). 50 years of computational wind engineering: Past, present and future. *Journal of Wind Engineering and Industrial Aerodynamics*, *129*, 69–102.

Blocken, B. (2015). Computational fluid dynamics for urban physics: Importance, scales, possibilities, limitations and ten tips and tricks towards accurate and reliable simulations. *Building and Environment*, *91*, 219–245.

Braun, A. L., & Awruch, A. M. (2009). Aerodynamic and aeroelastic analyses on the CAARC standard tall building model using numerical simulation. *Computers & Structures*, *87*(9), 564–581.

Dagnew, A. K., & Bitsuamlak, G. T. (2014). Computational evaluation of wind loads on a standard tall building using LES. *Wind and Structures*, *18*(5), 567–598.

Elshaer, A., Aboshosha, H., Bitsuamlak, G., El Damatty, A., & Dagnew, A. (2016). LES evaluation of wind-induced responses for an isolated and a surrounded tall building. *Engineering Structures*, *115*, 179–195.

Gowda, L., & Sitheeq, M. (1993). Interference effects on the wind pressure distribution on prismatic bodies in tandem arrangement. *Indian Journal of Technology*, *31*(7), 485–495.

He, B. J., Yang, L., & Ye, M. (2014). Strategies for creating good wind environment around Chinese residences. *Sustainable Cities and Society*, *10*, 174–183.

Huang, P., Luo, P., & Gu, M. (2005). *Pressure and forces measurements on CAARC standard Tall building in wind tunnel of Tong Ji University*. In Proceedings of the 12th national wind engineering conference of China, Xi'an, China (pp. 240–244).

Huang, S., Li, Q. S., & Xu, S. (2007). Numerical evaluation of wind effects on a tall steel building by CFD. *Journal of Constructional Steel Research*, *63*(5), 612–627.

Hui, Y., Tamura, Y., & Yoshida, A. (2012). Mutual interference effects between two high-rise building models with different shapes on local peak pressure coefficients. *Journal of Wind Engineering and Industrial Aerodynamics*, *104-106*, 98–108.

Kim, W., Tamura, Y., & Yoshida, A. (2011). Interference effects on local peak pressures between two buildings. *Journal*

of Wind Engineering and Industrial Aerodynamics, *99*(5), 584–600.

Kim, Y. C., & Kanda, J. (2013). Wind pressures on tapered and set-back tall buildings. *Journal of Fluids and Structures*, *39*, 306–321.

Kwon, D. K., & Kareem, A. (2013). Comparative study of major international wind codes and standards for wind effects on tall buildings. *Engineering Structures*, *51*, 23–35.

Lam, K. M., Leung, M. Y. H., & Zhao, J. G. (2008). Interference effects on wind loading of a row of closely spaced tall buildings. *Journal of Wind Engineering and Industrial Aerodynamics*, *96*(5), 562–583.

Li, Z., Sun, Y., Huang, H., Chen, Z., & Wei, Q. (2010). Experimental research on amplitude characteristics of wind loads of super tall buildings in hilly terrain field. *Journal of Building Structures*, *6*, 171–178.

Lin, N., Letchford, C., Tamura, Y., Liang, B., & Nakamura, O. (2005). Characteristics of wind forces acting on tall buildings. *Journal of Wind Engineering and Industrial Aerodynamics*, *93*(3), 217–242.

Liu, X. P., Niu, J. L., Kwok, K. C. S., Wang, J. H., & Li, B. Z. (2010). Investigation of indoor air pollutant dispersion and cross-contamination around a typical high-rise residential building: Wind tunnel tests. *Building and Environment*, *45*(8), 1769–1778.

Melbourne, W. H. (1980). Comparison of measurements on the CAARC standard tall building model in simulated model wind flows. *Journal of Wind Engineering and Industrial Aerodynamics*, *6*(1–2), 73–88.

Montazeri, H., & Blocken, B. (2013). CFD simulation of wind-induced pressure coefficients on buildings with and without balconies: validation and sensitivity analysis. *Building and Environment*, *60*, 137–149.

Murakami, S., & Mochida, A. (1988). 3-D numerical simulation of airflow around a cubic model by means of the k-ε model. *Journal of Wind Engineering and Industrial Aerodynamics*, *31*(2), 283–303.

Murakami, S., Mochida, A., & Hibi, K. (1987). Three-dimensional numerical simulation of air flow around a cubic model by means of large eddy simulation. *Journal of Wind Engineering and Industrial Aerodynamics*, *25*(3), 291–305.

Obasaju, E. D. (1992). Measurement of forces and base overturning moments on the CAARC tall building model in a simulated atmospheric boundary layer. *Journal of Wind Engineering and Industrial Aerodynamics*, *40*(2), 103–126.

Ramponi, R., & Blocken, B. (2012). CFD simulation of cross-ventilation for a generic isolated building: impact of computational parameters. *Building and Environment*, *53*, 34–48.

Richards, P. J., & Hoxey, R. P. (2006). Flow reattachment on the roof of a 6m cube. *Journal of Wind Engineering and Industrial Aerodynamics*, *94*(2), 77–99.

Spalding, D. B. (1972). A novel finite difference formulation for differential expressions involving both first and second derivatives. *International Journal for Numerical Methods in Engineering*, *4*(4), 551–559.

Stathopoulos, T., & Baskaran, B. A. (1996). Computer simulation of wind environmental conditions around buildings. *Engineering Structures*, *18*(11), 876–885.

Tanaka, H., Tamura, Y., Ohtake, K., Nakai, M., & Kim, Y. C. (2012). Experimental investigation of aerodynamic forces and wind pressures acting on tall buildings with various unconventional configurations. *Journal of Wind Engineering and Industrial Aerodynamics*, *107-108*, 179–191.

Tominaga, Y., Mochida, A., Yoshie, R., Kataoka, H., Nozu, T., Yoshikawa, M., & Shirasawa, T. (2008). AIJ guidelines for practical applications of CFD to pedestrian wind environment around buildings. *Journal of Wind Engineering and Industrial Aerodynamics*, *96*(10), 1749–1761.

Tsang, C. W., Kwok, K. C. S., & Hitchcock, P. A. (2012). Wind tunnel study of pedestrian level wind environment around tall buildings: Effects of building dimensions, separation and podium. *Building and Environment*, *49*, 167–181.

Yu, X. F., Xie, Z. N., Zhu, J. B., & Gu, M. (2015). Interference effects on wind pressure distribution between two high-rise buildings. *Journal of Wind Engineering and Industrial Aerodynamics*, *142*, 188–197.

Yuan, C., Ng, E., & Norford, L. K. (2014). Improving air quality in high-density cities by understanding the relationship between air pollutant dispersion and urban morphologies. *Building and Environment*, *71*, 245–258.

Zhang, A., & Gu, M. (2008). Wind tunnel tests and numerical simulations of wind pressures on buildings in staggered arrangement. *Journal of Wind Engineering and Industrial Aerodynamics*, *96*(10), 2067–2079.